Composites Part B 280 (2024) 111494

Contents lists available at ScienceDirect

Composites Part B

journal homepage: www.elsevier.com/locate/compositesb

Composite material based on piezoelectric core-shell nanofibers for tactile recognition

Giacomo Selleri [a,*], Filippo Grolli [a], Maria Roberta Randi [c], Emanuele Maccaferri [d], Tommaso Maria Brugo [b], Giovanni Valdrè [c], Andrea Zucchelli [b], Davide Fabiani [a]

[a] Department of Electrical, Electronic, and Information Engineering, University of Bologna, Viale Risorgimento 2, 40136, Bologna, Italy
[b] Department of Industrial Engineering, University of Bologna, Viale Risorgimento 2, 40136, Bologna, Italy
[c] Department of Biological, Geological, and Environmental Sciences University of Bologna, Via Zamboni 33, 40126, Bologna, Italy
[d] Department of Industrial Chemistry "Toso Montanari", University of Bologna, Viale Risorgimento 4, 40136, Bologna, Italy

ARTICLE INFO

Handling Editor: Prof. Ole Thomsen

Keywords:
Core-shell nanofibers
Piezoelectric
Self-sensing material
Impact localization

ABSTRACT

In recent years, self-sensing composite materials based on the direct piezoelectric effect have attracted widespread interest as they combine the composite material's mechanical performances with the piezoelectric phase's sensing capability. In this context, piezoelectric nanofibers exhibit minimal impact on the mechanical structure of the composite – differently from bulky films or ceramic disks - and represent a promising strategy for robotic applications or wearable devices. This work aims to develop a self-sensing laminate based on piezoelectric core-shell nanofibers (PEDOT:PSS-based core and P(VDF-TrFE)-based shell). Each layer of the laminate is made of a flexible epoxy material and embeds aligned nanofibers. By orthogonally overlapping two layers, the intersection points of the matrix-like arrangement of the nanofibers generate a network of piezoelectric pixels, which are responsible for sensing. Such a self-sensing composite material exhibited a noticeable capability to recognize the exact position of a mechanical stimulus on its surface.

1. Introduction

In the last period, the increasing diffusion of artificial intelligence and robotic systems has led to a rapid growth of innovative materials that combine their mechanical properties with other functionalities [1]. Many efforts have been made in mechanical engineering to integrate composite materials with sensors that can provide information about their status, such as deformations or mechanical impacts [2]. Moreover, the development of increasingly intelligent robotic systems (i.e., robotic hands or transfemoral prostheses) is giving rise to a generation of flexible devices that can interpret and dynamically interact with the surrounding objects [3,4]. Various stretchable and flexible pressure sensors – called electronic skins (e-skins) – have been developed according to different working principles [5–7]. Among these, the piezoresistive e-skins measure the change of the electrical resistance of a specific material as a consequence of an applied pressure. Their working depends on the intrinsic resistivity of the material, and improved sensing performances can be achieved by inserting nano additives into the polymeric matrix, such as carbon nanotubes [8] or graphene [9].

On the other hand, pressure sensors based on the capacitive effect convert the mechanical pressure into a variation of the capacitance. The sensitivity of such sensors strongly depends on the Young's modulus of the material used for their manufacturing [10,11]. However, the resistive and capacitive sensors require a power supply for their work, thus causing issues with battery replacement, especially in the case of remote-located sensors. The piezoelectric materials overcome this problem, as their transducing mechanism is intrinsically correlated with the non-centrosymmetric configuration of their crystal lattice. When an external stress is applied to the piezo material, the electric dipoles of the crystal get oriented, and electric charges are generated on the two opposite surfaces of the material. This principle is crucial in developing smart materials with intrinsic sensing capability without an external power supply [12]. Various piezoelectric composite materials have been designed and fabricated in the last decade, but the piezoelectric layer's interleaving negatively impacts the device's mechanical properties [13]. For this reason, the use of nanostructured piezoelectric materials (such as nano-powder [14] or nanofibers [15]) is paving the way for a class of self-sensing composite materials with negligible or no impacts on their

* Corresponding author.
E-mail address: giacomo.selleri2@unibo.it (G. Selleri).

https://doi.org/10.1016/j.compositesb.2024.111494
Received 23 February 2024; Received in revised form 11 April 2024; Accepted 21 April 2024
Available online 23 April 2024

mechanical properties [16,17]. Tactile sensors based on piezoelectric nanofibers have recently attracted widespread attention because of their high sensitivity and the self-powering capability of piezoelectric polymers such as poly(vinylidene fluoride) (PVDF) and its copolymer poly (vinylidene fluoride-trifluoro ethylene) (P(VDF–TrFE)) [18,19]. Several works in the literature report on the realization of flexible pressure sensors embedding PVDF nanofibers in a soft polymeric matrix [20–22]. Electrospinning is a consolidated technique for preparing nanofibrous materials, which allows the production of polymeric nanofibers by high-voltage electrostatic extrusion of a polymeric solution when placed on a sharp edge [23]. The high voltage applied during the electrospinning induces a mechanical stretching of the polymeric jet, which is beneficial for forming the β phase, responsible for the piezoelectric behavior of PVDF [24,25]. The randomly oriented PVDF and P (VDF-TrFE)-based nanofibrous layers were used in the robotic field (i.e., development of electronic skins [5]) or wearable applications [26]. Despite the valuable effect of the electrospinning process on the piezo-properties of the nanofibers, a subsequent polarization process is generally required to align the ferroelectric dipoles of the material, thus enhancing the piezoelectric response of the layer ([27–30]). Besides the polarization process, other strategies to enhance the piezoelectric response of the nanofibers were investigated in the literature. The pressure sensitivity and the ability to generate electric charge of the PVDF fibers increase when they are more aligned in one direction [31]. Various methods were developed to achieve this alignment for the nanofibers. For example, Edmondson et al. proposed a technique that combines parallel-electrode electrospinning and centrifugal dispersion to produce highly aligned and uniform nanofibers. They showed how the degree of fiber alignment affects the voltage production capacity [32]. The influence of different rotation speeds of the disk collector during the electrospinning process was investigated in relation to the alignment level of the nanofibers and the β phase orientation in the polymer chains [33]. Sensors with 80 % of aligned fibers produced signals with amplitudes about four times higher than those with only 30 % [34]. The nanofibrous layers were made more sensitive by adding nanofillers, such as Ag nanowires and multi-walled carbon nanotubes, increasing the β phase content in the crystalline structure [35]. Another significant improvement in sensitivity was achieved by using aligned core–shell nanofibers of P(VDF-TrFE) made by electrospinning. The sensitivity values (up to 4000 μV/mmHg) of P(VDF-TrFE) nanofibers were four times higher when they were arranged in an aligned array with a conductive core (PVP-PEDOT:PSS) and a piezoelectric shell (P (VDF-TrFE)). These sensitive membranes were applied to create pressure sensors for endovascular use [36].

The innovative self-sensing technique of the proposed laminate consists of incorporating self-powered micro-pixels inspired by the skin sensing principle. The laminate comprises nanostructured wires embedded within a flexible matrix and aligned with each other. These sensing wires are comprised of core-shell piezoelectric nanofibers. The composite is formed by overlapping at least two layers, with the nanostructured wires arranged perpendicularly. The cross-points of the wires represent the micro-pixels responsible for sensing. Semiconductive flexible electrodes connect the edges of the composite's individual layers to the measurement instrumentation to extract piezoelectric signals from each pixel. The simplicity of construction, sensibility, and accuracy with which the new material can sense impacts and shocks are presented in the paper. These characteristics make the material especially suitable for soft robotics, biomedical, textiles, and industrial automation applications.

2. Materials and methods

This section illustrates the manufacturing steps for the fabrication of the piezoelectric sensor. Section 2.1 and Section 2.2 strongly focus on producing high-quality core-shell nanofibers, as they play a crucial role in the sensor working mechanism. The electrospinning parameters and the polymeric solution concentrations (both for the core and the shell) have been accurately tuned to ensure coaxial morphology. Afterward, the sensor fabrication and electromechanical characterization are reported in Section 2.3 and Section 2.4, respectively.

2.1. Polymeric solutions preparation

The interaction between the core and the shell polymeric solutions is a critical parameter for high-quality nanofiber production. When the droplet is charged at a sufficiently high electric field, it emits a charged jet with the liquids coaxially arranged within the jet. The evaporation rate of the volatile solvents of the liquid solutions depends on different factors (i.e., solvents boiling point, solutions concentrations, distance from the ground collector) and determines the coaxial morphology of the solid fibers [37]. A successful process depends on the design of the two polymeric solutions so that the electrospinning process and the solidification of the fibers happen in the desired manner. In this section, the preparation of different core and shell solutions has been studied by varying their solvent concentrations and thus their viscosity. The aim is to precisely tailor the nanofibers' morphology by controlling the solutions' viscosity values and to identify the parameters for producing smooth and beads-free coaxial nanofibers in a stable electrospinning process.

2.1.1. Shell polymeric solutions

For the shell solution, P(VDF-TrFE) Solvene (75/25%mol, Mw = 410 kDa), kindly provided by Solvay Specialty Polymers (Bollate, Italy), was dissolved in methylethylketone (MEK) and dimethylformamide (DMF) (Sigma Aldrich). The solvents were fixed in a 72:28%wt proportion, MEK and DMF respectively. The piezoelectric polymer concentration was varied from 18%wt to 28%wt to produce six shell polymeric solutions (S1–S6), as reported in Table 1. Each solution was left on a magnetic stirrer at 40 °C for 40 min before the electrospinning.

2.1.2. Core polymeric solutions

The conductive polymer poly(3,4-ethylenedioxythiophene) doped with poly(styrene sulfonate) anions (PEDOT:PSS dissolved in water in a concentration of 3–4%, as provided by Sigma Aldrich, with a viscosity equal to 10–30 mPa*s) was used as the core of the nanofibers. The polymeric solutions were prepared by dissolving the PEDOT:PSS in DMF. Polyvinylpyrrolidone (PVP) was added as a carrier polymer and solution viscosity modifier, creating a solution based on PEDOT:PSS and PVP. The PVP concentration was varied from 2.9%wt to 6.1%wt to prepare three core solutions (C1–C3), as reported in Table 2. Moreover, a PEDOT:PSS dissolved in 5 % in water, as provided by Sigma Aldrich, was used to produce seven core solutions, both with PVP and without. Compared with the PEDOT:PSS used for C1–C3 solutions, the higher concentration of this PSS results in higher conductivity, a viscosity of 30–90 Pa*s, and a gel physical state. The higher viscosity of the PEDOT:PSS dissolved in 5 % in water allowed the production of polymeric solutions ready for electrospinning without adding PVP. However, some polymeric solutions were still prepared with PVP (C8–C10). All the polymeric solutions used for the core are reported in Table 2.

Table 1
Shell polymeric solutions based on P(VDF-TrFE) different concentrations.

(%wt)	P(VDF-TrFE)	DMF	MEK
S1	18 %	23.0 %	59.0 %
S2	20 %	22.5 %	57.5 %
S3	22 %	21.8 %	56.2 %
S4	24 %	21.3 %	54.7 %
S5	26 %	20.7 %	53.3 %
S6	28 %	20.1 %	51.9 %

Table 2
Core polymeric solutions based on PEDOT:PSS.

		PEDOT:PSS (% wt)	DMF (% wt)	PVP (% wt)
PEDOT:PSS (3–4% in water)	**C1**	20.2 %	76.9 %	2.9 %
	C2	20.2 %	75.4 %	4.4 %
	C3	20.2 %	73.7 %	6.1 %
PEDOT:PSS (5 % in water)	**C4**	60 %	40 %	/
	C5	50 %	50 %	/
	C6	45 %	55 %	/
	C7	40 %	60 %	/
	C8	44 %	50 %	6 %
	C9	42 %	53 %	5 %
	C10	36 %	60 %	4 %

2.2. Electrospinning process

The electrospinning process took 15 min, and 50 μm thickness nanofibrous mats were produced for each core-shell solutions combination described in Section 2.1. The randomly oriented nanofibers were collected on a ground plane collector, and each sample was analyzed in terms of the stability of the electrospinning process and coaxial morphology of the nanofibers. The setup parameters of the electrospinning process were adjusted for each core-shell solutions pair in order to achieve a stable configuration of the Taylor cone and avoid liquid leakage from the needle.

The distance between the needle and the ground collector was varied from 10 cm to 16 cm, and the high voltage value was set from 9 kV up to 16 kV, depending on the properties of each polymeric solution. In general, higher electric field values are required for more viscous solutions as the droplet's surface tension has a dominant role. The flow rate of the shell solution was equal to 1.1 mL/h, and the core solution was equal to 0.35 mL/h. The coaxial needle has an inner diameter of 0.8 mm, and the outer one equals 1.2 mm. The room temperature was 25 °C for all the tests, and the chamber moisture was set at 40 %.

2.3. Sensor manufacturing

The core-shell polymeric solutions pair that produced the best quality core-shell nanofibers were identified and exploited for sensor manufacturing. The sensor working principle is based on the direct piezoelectric effect, as schematically represented in Fig. 1. As a mechanical impact is applied on a single nanofiber, the piezoelectric shell generates a charge distribution on its opposite surfaces (inner part and outer part). Hence, by covering the outer part of the shell with a metal coating, it is possible to realize a coaxial nano-piezoelectric sensor, where the opposite polarity charges are collected by the inner conductive core and the outer metalized layer, thus generating a voltage difference, as shown in Fig. 1.

The nanofibers are aligned and integrated into the epoxy matrix to fabricate the first layer of the sensor. The second layer of the laminate is

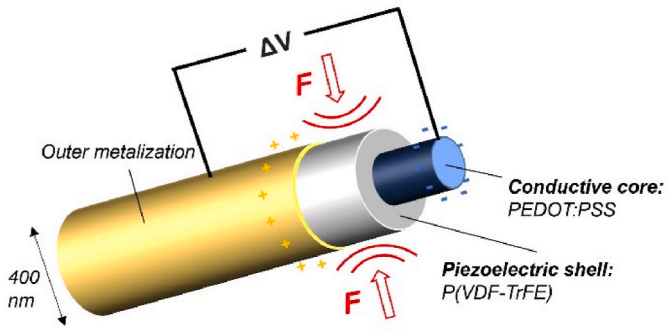

Fig. 1. Schematic configuration of the core-shell nanofiber.

then added so that the nanofibers are orthogonal to those of the first one as if they were arranged in a matrix-like disposition (rows-columns). The cross-points of the nanofibers represent the sensitive pixels that make the laminate sensitive all over its surface. Suppose an impact occurs on the sensor surface. In that case, the amplitude of the output voltage correlated to the impacted pixel should be the highest if compared with the voltages referring to the non-impacted ones. The output voltage is measured by electrically connecting the core (core signal) and the outer metallization (shell signal) to an acquisition system. However, due to the nanometric scale of the connections, it is challenging to acquire the electrical signals generated by every nanofiber.

Nevertheless, a proof-of-concept to demonstrate the working principle of such a sensor can be done by electrically connecting multiple nanofibers using macroscale electrodes, as this work aims to do. For instance, in the schematic representation of Fig. 2, the nanofibers are grouped in three rows and three columns, thus creating a surface with nine sensitive pixels. The macroscale electrodes for the shell and the core signals collection are disposed on the opposite edges of the sensor, and their electrical contact with the nanofibers (e.g., connections with the core and with the outer metallization) can be seen in the red magnification panels of Fig. 2. In the case of the shell electrode, the aim is to surround the nanofibers with the macroscale electrode without any contact with the core. To ensure adequate contact between the electrodes and the nanofibers, traditional metallic electrodes such as brass sheets or aluminum foils are unsuitable, as they cannot surround the cylindrical shape of each nanofiber and could rip in case of bending. Therefore, semiconductive materials may be fabricated by adding conductive nanoparticles to the epoxy matrix (i.e., carbon nanotubes or carbon black nanoparticles) to make the embedding medium electrically conductive. In this way, the semiconductive epoxy matrix can surround the whole structure of the nanofiber and electrically connect the outer metalized portion of the nanofiber during the curing process. Similarly, the core signals were collected by curing the semiconductive material on the smooth edge of the sensor, where the cores of the nanofiber face (see magnification panel of Fig. 2). The nanofibers' last portions are not metalized to avoid electrical contact between the core and the outer metallization. The output voltage for each group of nanofibers is then measured as a voltage difference between the inner cores and the shell for each group of nanofibers, which compose the nine sensitive pixels of the sensor surface. The exact position of a mechanical impact on the surface of the sensor is detected by comparing the output voltages of each group of nanofibers and going back to the corresponding positions. In the case of an impact in the center of the sensor – as shown in Fig. 2 – the highest output voltages would be ΔV_5 and ΔV_2. Consequently, the resolution of the impact localization strongly depends on the number of core electrodes stacked on the sensor's edge, which determines the number of sensitive pixels. The higher the number of core electrodes, the higher the precision of the impact localization. Ideally, if it was possible to distinctly acquire the signal of every single nanofiber, this sensor could recognize the impacted position with nanometric precision. In this work, a flexible sensor with 3 x 3 sensing positions has been fabricated. The manufacturing steps of the flexible sensor are described in this section and schematically represented in Fig. 5.

2.3.1. Aligned coaxial electrospinning

The electrospinning process apparatus used to produce aligned coaxial nanofibers is represented in Fig. 3. The alignment process of the nanofibers was electrically induced by using two copper wire electrodes parallelly disposed at 7 cm distance from each other. In this way, the liquid jet in the whipping zone is influenced by the two parallel ground electrodes and the coaxial nanofibers solidify perpendicularly to their direction. Such an alignment mechanism preserves the geometrical structure of the nanofibers, contrary to mechanical alignment methods (i.e., high-speed rotating drum collectors [38]) that could damage their coaxial morphology. The coaxial electrospinning process took place for 5 min to produce a thin layer of aligned coaxial nanofibers. A translation

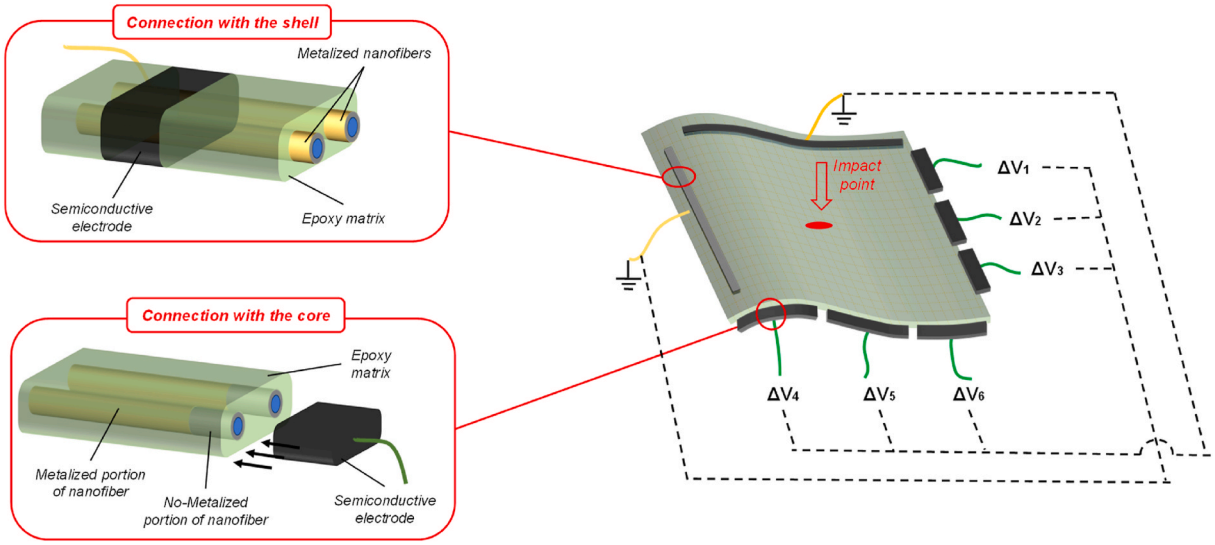

Fig. 2. Schematical representation of the core-shell nanofiber-based sensor.

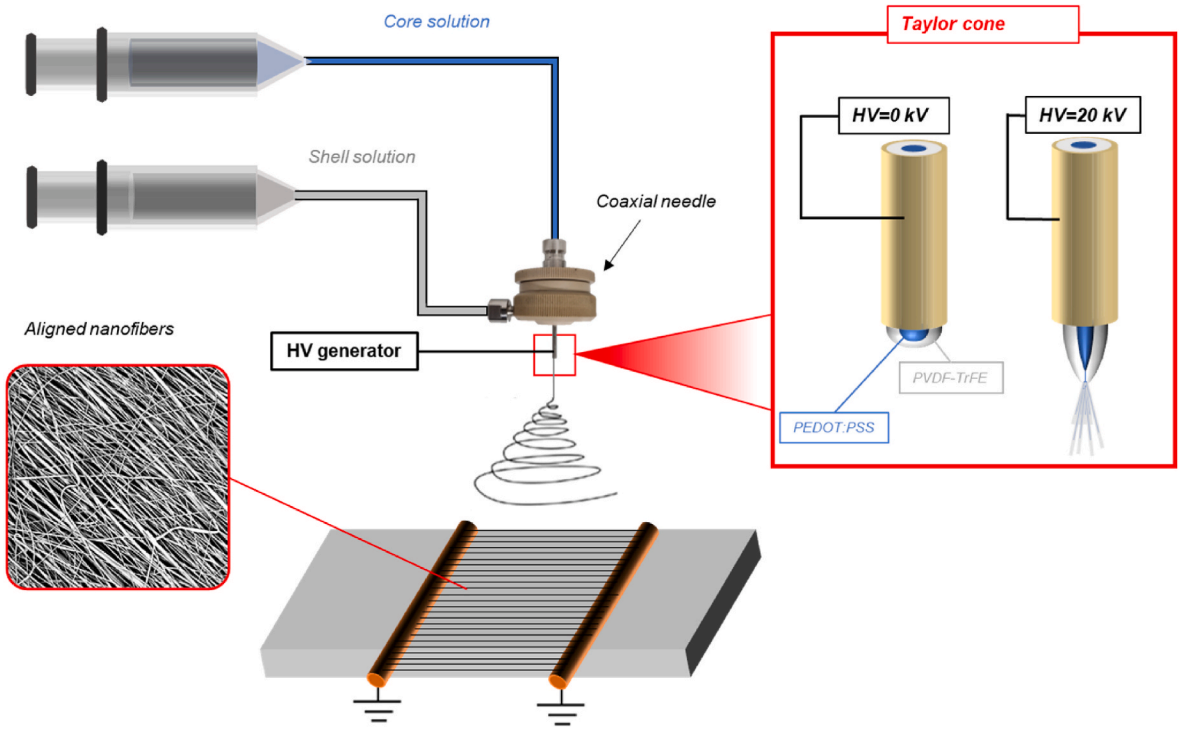

Fig. 3. Electrospinning apparatus for aligned core-shell nanofibers.

movement was imposed on the structure of the ground collector in order to have a uniform distribution of the nanofibers along the length of the grounded wires.

2.3.2. Shell electrodes

Considering a group of aligned nanofibers (Fig. 5a), the electrical charges generated by the piezoelectric shell accumulate on their outer part. Therefore, the nanofibers were sputter-coated with gold (Quorum SC7620 Sputter Coater) to create a nanoscale external electrode. The final part of the nanofibers (1 cm length) was not metalized to avoid electric contact between the core and the outer metallization (Fig. 5b). As previously explained in Fig. 2, a single macroscale electrode has to be connected to the metalized portion of the nanofibers for signal acquisition. For this purpose, the use of traditional metallic electrodes such as aluminum foils or copper tapes could not be effective, as the nanofibers could move or not totally be in contact with them. With the aim to guarantee flexibility to the sensor and avoid any mechanical discontinuities, carbon black (CB) nanoparticles were adopted to realize the electrodes. If the CB nanoparticles are mixed into a polymer matrix, their high specific surface area can form a conductive network, which significantly increases the conductivity of the resin, even by mixing a low amount of nanoparticles [39,40]. When embedding the nanofibers within a semiconductive polymeric matrix, the whole surface of each nanofibers is surrounded, and the electrical contact is guaranteed.

In this work, CB nanoparticles (Printex XE2B, BET surface area = 1000 m2/g, average particle size = 30 nm) were dispersed in a soft polymeric matrix. The soft matrix consists of a mixture of epoxy resin (Itapox 108, kindly provided by Ddchem S.l.r., Verona, Italy) and

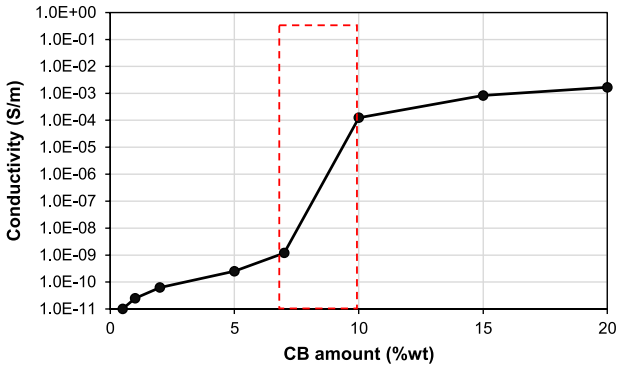

Fig. 4. Electrical conductivity of the semi-conductive layers as function of the CB content.

blocked isocyanate polyurethane prepolymer (Synthane 2095, Synthesia Technology, Barcelona, Spain).

Before manufacturing the macroscale shell electrodes of the sensor, an experimental campaign was conducted by fabricating different layers with and varying the amount of CB content. The CB nanoparticles were added in different weight percentages to the aforementioned polymeric matrix in a range between 0.5 and 20 %wt. The liquid formulation was then prepared by adding 300%wt of isopropanol and magnetically stirred for 120 h at room temperature to uniformly disperse the CB nanoparticles in the solution. The curing agent (Itamine CA119, Ddchem S.l.r., Verona, Italy) was added and the mixture was heated at 50 °C to facilitate the isopropanol to evaporate. The curing process was then carried out for 2 h at 50 °C. The thickness of the produced layers was equal to 100 ± 12 μm, and the electrical conductivity was measured for all of them, as reported in Fig. 4.

As observable from the graph, the electrical conductivity of the layers gradually increases for a CB content between 0.5 and 7%wt. Afterward, for values higher than 7%wt, the conductivity sharply increases up to $1.25*10^{-4}$ S/m for a CB content equal to 10%wt. In that region, the percolation threshold is reached (red-dashed area of the graph of Fig. 4) and the CB nanoparticles created a conductive network, remarkably enhancing the electrical conductivity. Higher CB contents (i.e., 15 %wt and 20 %wt) strongly affected the curing process of the layers, thus worsening their mechanical properties (i.e., stretchability and flexibilities).

For these reasons, the macroscale shell electrodes of the sensor were manufactured by adding a CB content equal to 10 %wt. The pre-cured semiconductive mixture was deposited on a Teflon support, and before curing, the metalized edge of the nanofibrous mat was deposited on the uncured electrode. A further CB-based layer was deposited on it to create a sandwich-like structure for the electrical contact with the metalized part of the shell of the nanofibers. The gel-like consistency of the conductive polymeric matrix before the curing process allows an optimal embedding of the nanofibers and ensures electrical contact with the metalized shell of the nanofiber.

The same process was repeated for the other 90° oriented shell electrode, as shown in Fig. 5c. The curing process was performed at 50 °C for 2 h. Signal cables were added during the curing process.

2.3.3. Integration in a soft matrix

The central portion surface of the piezoelectric sensor was made by embedding the nanofibers in the same embedding medium described in Section 2.3.2, without the CB nanoparticles. Therefore, the polymeric mixture - composed of epoxy resin (55%wt), polyurethane (24%wt), and curing agent (21%wt) - was poured on the nanofibrous layer and cured for 2 h at 50 °C (Fig. 5d).

The choice of the same polymeric mixture both for the CB-based electrodes and for the embedding medium was made to achieve a good adhesion at the interface. Metallic electrodes such as copper wires or aluminum foils would limit the flexibility of the sensor as a consequence of their limited maximum strain before the break.

2.3.4. Core electrodes

The electric charges accumulated in the inner surface of the shell of the nanofibers flow through the conductive PEDOT:PSS-based core, which works as a nanometric electrode. At the macroscopic scale, the core of the nanofibers is electrically connected to CB-based electrodes, which are stacked at the edges of the sensor surface. Their composition is the same as used for the shell electrodes, as described in Section 2.3.2. Before their deposition, each non-metalized side of the sensor was broken in a nitrogen bath in order to have a smooth and clear cross-section area (Fig. 5e). Thus, the whole cross-section areas of the core of the nanofibers were exposed, and the CB-based solution was deposited on them to create the electrical contact (Fig. 5f). The curing process

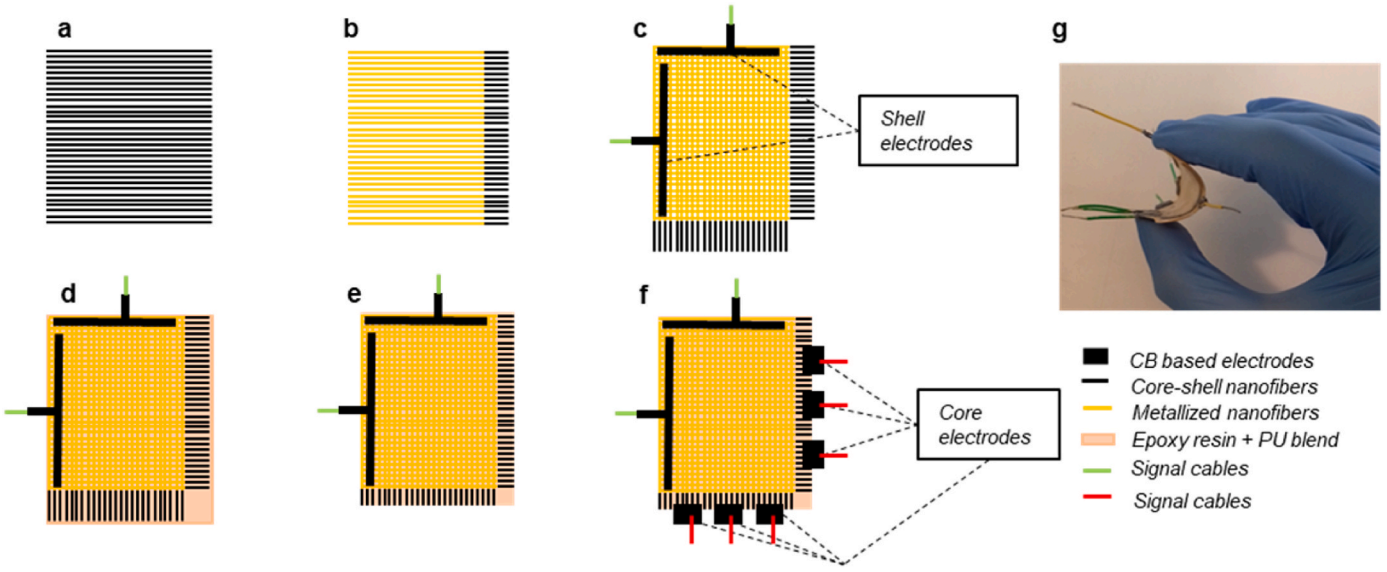

Fig. 5. (a) Aligned core-shell nanofibers; (b) partial metallization of the nanofibers; (c) CB-based electrodes for shell signal; (d) integration in soft hosting matrix; (e) fragile cut in nitrogen bath for the core exposing; (f) CB based electrodes for core signal; (g) final sensor.

was then carried out for 2 h at 50 °C, and signal cables were added.

As proof of concept, in this work, three core electrodes were designed for each side of the sensor, but higher precision in tactile sensing can be achieved by increasing their number.

2.4. Characterization techniques

2.4.1. Viscosity analyses

The viscosity of each polymeric solution was measured by means of an Anton Paar rheometer. The polymeric solution was placed on a horizontal plate, and a rotating cone was placed into it. The angle between the surface of the cone and the horizontal plate was equal to 1°. The cone worked at growing rotating speeds, thus making the liquid move. The viscosity was then measured for different velocity values. In particular, the viscosity value considered for this study corresponds to the velocity of the polymeric solutions when they flow out from the needle during the electrospinning process.

2.4.2. Nanofibers characterization

The crystallinity and the morphology of the core-shell nanofibers mats were characterized using a variety of methods. The morphology of the electrospun fibers was analyzed through a Phenom Pro X Scanning Electron Microscope (SEM). The SEM images from above the nanofibrous mats are used to monitor any discontinuities along the fiber axis or bead formations, and to measure the average diameter. The cross-section views of the nanofibrous layers are used to estimate the coaxial shape of the nanofibers in the observed point, and to measure the thickness of the shell. In this case, the nanofibrous layers were previously cut in a nitrogen bath to have a fragile break of the fibers, thus leading to a smooth cross-section. Afterward, the mats were soaked for 30 min in a distilled water bath to dissolve the PEDOT:PSS-based core. In this way, the hollow fibers visible in the SEM images represent the previous core-shell nanofibers. Furthermore, the morphology of the produced nanofibers was observed by means of a Transmission Electron Microscope Philips TEM CM 100 at an electron accelerating voltage of 80 kV. The TEM micrograph analyses were performed with the aim to investigate at high spatial resolution the coaxial shape of the nanofiber along its length. In the TEM images (Section 3.2), the dark portion of the nanofibers corresponds to the conductive polymer (PEDOT:PSS-based core), whereas the light grey one refers to the piezoelectric shell of P(VDF-TrFE).

To investigate the fraction of the β phase, the one responsible for the piezoelectric behavior, the characteristic absorption bands the Infrared Spectra were performed by using a Fourier transform infrared spectrometer (FTIR, PerkinElmer UATR Two) in the range between 600 and 1600 cm^{-1} range. Moreover, the crystallinity X-ray diffraction (XRD) measurements were carried out using an X'PERT pro Instrument, with detector 1-D PIXcell using Cu radiation 1.54 Å. For comparison, FTIR and XRD tests were also performed on a P(VDF-TrFE) (75/25%mol, M_w = 410 kDa) nanofibrous mat, appositely manufactured via electrospinning.

2.4.3. Electromechanical characterization

The electromechanical tests were performed on the piezoelectric sensor to verify its capability to recognize the position of a mechanical impact on its surface. As shown in Fig. 6, the nanofibrous piezoelectric sensor was fixed on a support placed over a 300 N capacity load cell (Model 1042, Single point load cells, Tedea-Huntleigh). The slider initial position of a linear motor (LinMot) was fixed such in a height that the amplitude of the impact force on the piezoelectric sensor was equal to 100 N. The indenter has a diameter equal to 1 cm. The impact position on the surface of the sensor was varied in all the nine sensitive pixels of the 3x3 matrix and the output piezoelectric signals of the shell and core electrodes were simultaneously acquired by means of a digital oscilloscope (Tektronix DPO 5034). The comparison between the magnitude of the output voltages gives an estimate of the impacted position. To monitor eventual contribution of the triboelectric effect on the piezoelectric output voltage, the electromechanical tests have been repeated on an additional composite laminate (named as virgin laminate), which was fabricated with the same procedure described in Section 2.3, but with no nanofibers interleaved (Section S3 of Supplemetary Materials).

3. Results and discussion

The viscosity values of the polymeric solutions used for the core and for the shell of the nanofibers are reported in Section 3.1, and their impact on the morphology of the coaxial nanofibers obtained via electrospinning is evaluated through micrograph analyses of Section 3.2. Finally, in Section 3.3 the impact localization capability of the sensor is reported.

3.1. Polymeric solutions viscosity

The shell solutions' viscosities are reported in Fig. 7a, and the core solutions ones are reported in Fig. 7b both for the PEDOT:PSS dissolved in water at 3–4% and for PEDOT:PSS dissolved in water at 5 %. The higher the concentration of P(VDF-TrFE), the higher the viscosity of the shell solutions, whose maximum value is for the S6 solution (0.9 Pa*s). Considering the core polymeric solutions, the carrier polymer PVP strongly affects the viscosity values even for low variations (i.e., from 0.27 Pa*s of solution C10 to 2.2 Pa*s of solution C8).

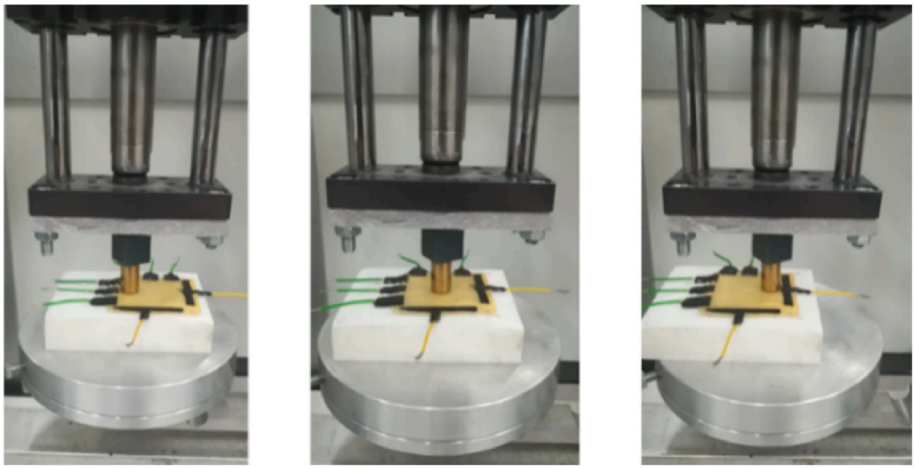

Fig. 6. Linear motor impacting the sensor in three different sensing positions.

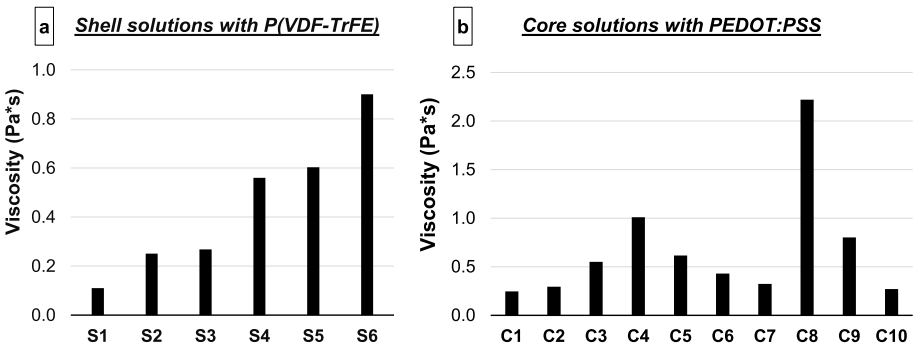

Fig. 7. Viscosity values of the a) shell solutions based on P(VDF-TrFE) and the b) core solutions based on PEDOT:PSS.

3.2. Micrograph and chemical analyses

The TEM and SEM micrographs of the most representative combinations between the core and the shell solutions are reported in this section and correlated with the viscosity measurements reported in the previous section. Each row of the panel corresponds to a specific combination of core and shell polymeric solutions, together with the respective viscosity values. The first column of the panel of Fig. 8 reports the SEM images of the nanofibers from the top view, whose average diameters $Ø_{nf}$ and standard deviation were measured on 100 fibers by using the software ImageJ. The hollow fibers can be seen in the SEM cross-sections of the second column, and the shell thickness t_{sh} was measured on the fibers directly facing the cut plane. Finally, in the TEM images of the third column of the panel the coaxial morphology of the nanofibers can be observed, and t_{sh} was also measured. It is worth highlighting that in TEM images, the black portions of the images correspond to conductive material (in this case, PEDOT:PSS), whereas the light grey portions of the nanofibers correspond to P(VDF-TrFE).

The first row of the panel (Fig. 8a) refers to the S1 and C1 combination, with a viscosity value equal to 0.11 Pa*s and 0.25 Pa*s, respectively. The top view SEM image of the nanofibrous layer presents nanofibers with coarse and not regular surfaces, resulting in a high standard deviation value of their average diameter ($Ø_{nf}$ = 915 ± 488 nm). The very low viscosity of the shell polymeric solution resulted in a leakage of the core outside of the shell, thus deforming the nanofibers into split emptied entanglements. The compromised coaxial shape can also be observed both in the cross-section SEM image, where most of the fibers appear flat and crumpled, and in the TEM image (third column of Fig. 8a), where the light grey (P(VDF-TrFE)) and the dark (PEDOT:PSS) portions are not coaxially arranged. In this case, the measurement of t_{sh} was not applicabile (N/A). The C4/S2 combination is observable in Fig. 8b. The coaxial morphology of this combination is not achieved as the core solution presents a very high viscosity value (1.01 Pa*s) with respect to the shell one (0.25 Pa*s). This aspect leads to the formation of enlargements of the fibers (top view and cross-section SEM images) in a way that the core fills up the totality of the fiber diameter (TEM image). Moreover, very few hollow fibers are visible in the SEM image of the cross-section of the nanofibrous layer of Fig. 8b. As consequence, t_{sh} was not measurable and $Ø_{nf}$ is very irregular. The third combination of the panel (Fig. 8c) presents a reversal of trend, as the viscosity of the shell solution S4 (0.56 Pa*s) is higher than the viscosity of the core solution C2 (0.29 Pa*s). In this case, smooth and beads-free nanofibers are visible in the SEM images of Fig. 8c, and the core leakage outside of the shell is not visible, as the viscosity of the shell solution S4 is considerably increased with respect to S1 and S2. The core is well confined inside the shell (TEM image), and a remarkable amount of hollow fibers is observable in the SEM cross-section view of Fig. 8c. However, high values of standard deviation are present both for $Ø_{nf}$ and t_{sh}, and the latter considerably differs if calculated in the SEM cross-section view or in the TEM image. Fig. 8d and e report the images of S4/C7 and S4/C10 combinations, respectively. The core solutions present very similar viscosity values (C7 = 0.3 Pa*s and C10 = 0.27 Pa*s). However, they differ in composition, as the C10 polymeric solution was made by adding 4% wt of PVP, and in the core solution C7 the PVP is absent. Similarly to Fig. 8c, no split fibers are present, and a remarkable amount of hollow fibers is visible in the SEM cross-section views of Fig. 8d and e. Moreover, the TEM images confirm the optimal coaxial shapes obtained with those viscosity values, as the cores are well-confined within the piezoelectric shells, both for the S4/C7 and S4/C10 combinations. In particular, the S4/C10 combination led to the production of nanofibers with $Ø_{nf}$ = 659 ± 90 nm, presenting the lowest standard deviation value among all the tests performed. Similarly, in the SEM cross-section view the measured shell thickness (t_{sh} = 241 ± 31 nm) has the lowest standard deviation value, and it is consistent with the t_{sh} measured in the TEM image. Consequently, for the self-sensing laminate manufactured in this work, the combination of core-shell polymeric solutions used for electrospinning was S4/C10 (High-Voltage applied to the needle equal to 14 kV and needle-ground distance equal to 12 cm). The FTIR and XRD analyses were performed on the core-shell nanofibers obtained via coaxial electrospinning with S4 and C10 polymeric solutions, as reported in Section S1 of Supplemetary Materials. Figure S1 shows an overlay of the IR spectra of the as-spun sample based on P(VDF-TrFE)/PEDOT:PSS core-shell nanofibers and the one with P(VDF-TrFE) nanofibers. According to literature, the peaks at 846, 1083, 1285 and 1431 cm^{-1} are the one related to the β phase [41–43], while the peak at 1123 cm^{-1} is related to the TrFE content [42]. The crystalline phase of the two nanofibrous mats is visible in the XRD patterns of Fig. S2. A prominent peak at 2Θ = 19.8° is visible, which is typically assigned to the β-crystal phase of P(VDF-TrFE). In the case of core-shell nanofibers (blue line), the shoulder centered around 17° is associated to the amorphous phase of PEDOT:PSS [44].

3.3. Electromechanical response

The piezoelectric core-shell nanofiber-based sensor was electromechanically characterized as described in section 2.4.3. The edges of the sensor equipped with the three core electrodes provide a surface with nine sensitive pixels. The indenter impact position was varied to mechanically stress all the pixels on the sensor's surface, and the piezoelectric signal was simultaneously acquired for each electrode.

As the indenter impacts one of the nine available positions with a force of 100 N, the three signal amplitudes of the electrodes stacked on each side of the sensor are compared. The output signals with the highest amplitudes provide the coordinates to recognize the position of the sensor surface where the impact occurred. Each core electrode was labeled (i.e., electrodes A, B and C for one side and electrodes D, E and F for the other side), and each pixel was numbered as shown in Fig. 9. For instance, Fig. 9 reports the output piezoelectric signals measured for an impact occurring on the pixel in the center of the sensor (red circle, Pixel 5). The signal amplitude ΔV_B, which refers to the central pixel, exceeds

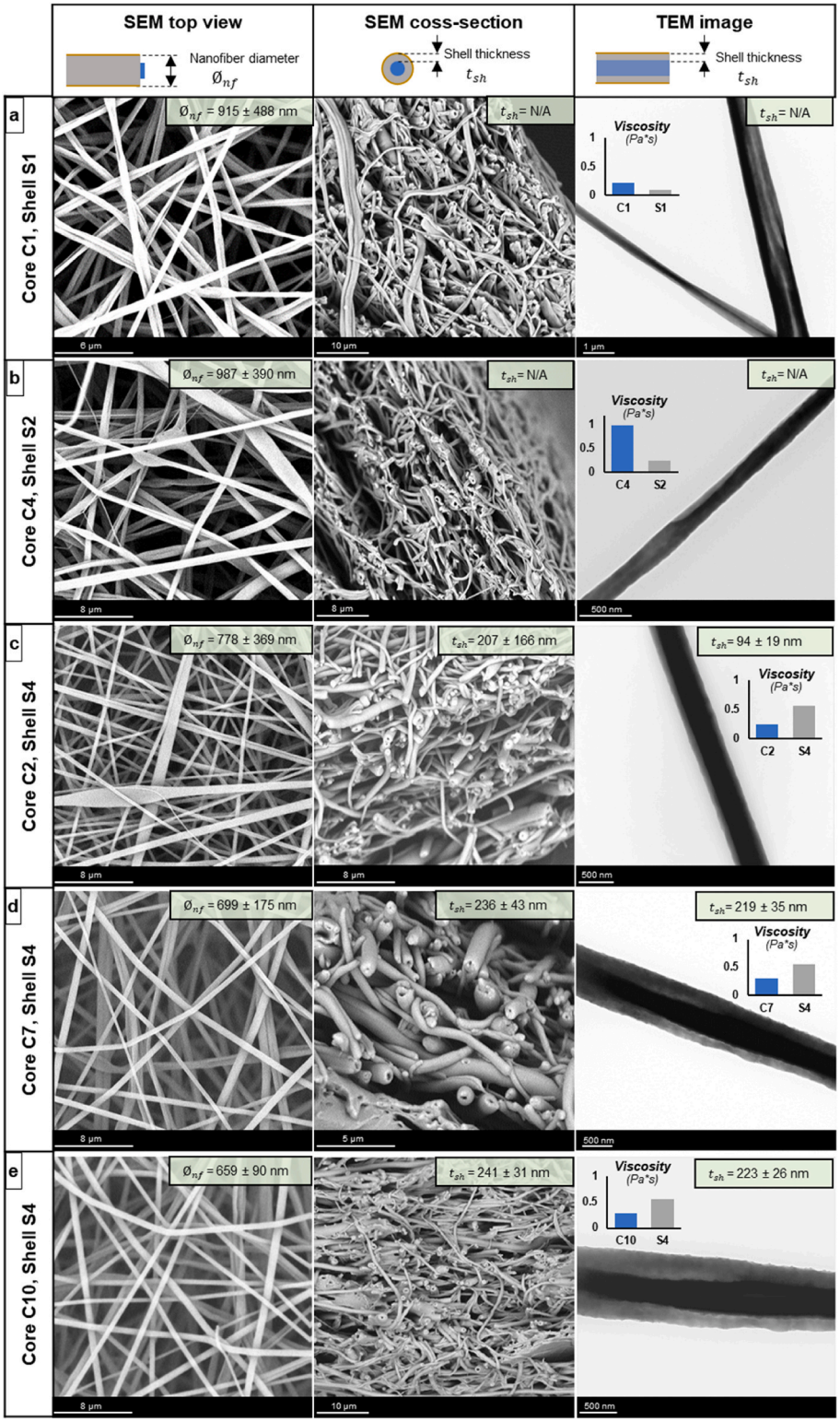

Fig. 8. SEM and TEM images of the core-shell nanofibers electrospun from different polymeric solutions, along with the measurement of the diameter $Ø_{nf}$ and the thickness of the shell t_{sh}.

the other piezoelectric signal amplitudes of the corresponding belonging side. Similarly, ΔV_E is higher than ΔV_D and ΔV_F. As a consequence, it can be assumed that the mechanical impact occurred in the intersection between the row of electrode_B and the column of electrode_E, i.e., the central pixel of the sensor surface.

Similarly, the mechanical impacts were performed on the nine sensing positions of the sensor. For each impacted pixel, Fig. 10 reports the piezoelectric signal amplitudes (calculated as the peak-to-peak value) as the average value of the three repetition, along with the corresponding standard deviation. The dashed circles on the surface of the sensor represent the nine sensing pixels, and the red one indicates the position of the mechanical impact. The position of the impact is obtained

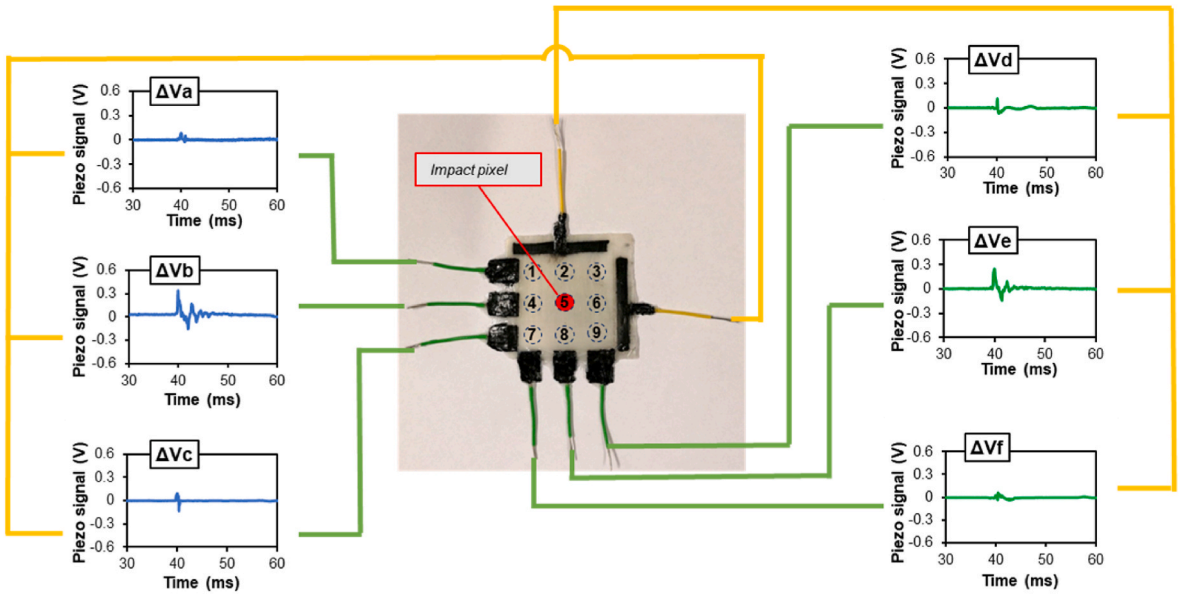

Fig. 9. Output voltages of the electrodes in the case of an impact in the center of the sensor.

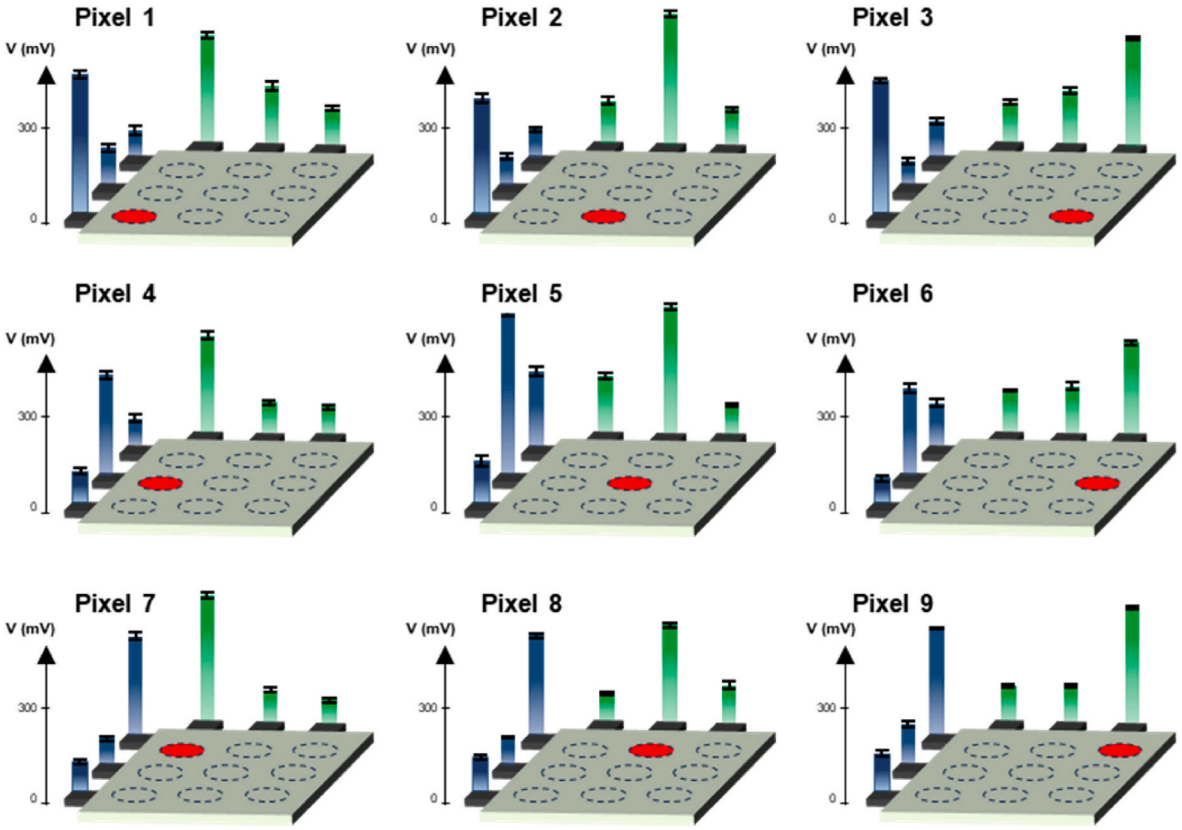

Fig. 10. Piezolectric output voltages of each electrode measured for nine different impact positions.

by comparing the output voltages measured on the electrodes at the edges of the sensor, i.e., the signals ΔV_A, ΔV_B, ΔV_C, and the edge with electrodes ΔV_D, ΔV_E, ΔV_F. Crossing the row and the column with the highest amplitudes makes it possible to identify the sensing pixel where the impact occurred. The piezoelectric output voltages values are also reported in Table S1 (see Supplementary Materials) for the nine impact positions and the highest piezoelectric output is boldly highlighted for each electrode row. The electric signals of each electrode are reported as the average of the three repetitions performed on each pixel, together with the corresponding standard deviation, as reported in Section S2 of Supplementary Materials. Overall, the positions of the impacts were correctly identified for all nine positions. The highest output voltages were always measured on the electrodes referring to the mechanically stressed pixel, thus validating such an impact localization technique. Nevertheless, variations in the amplitude of voltage outputs are evident across different impacted positions and two primary factors contributing

to this phenomenon can be discerned. Firstly, the non-uniform distribution of nanofibers on the sensor surface may result in areas of heightened sensitivity as well as less responsive regions. Additionally, an uniformly sensitive area of the sensor is the result of an ideal coaxial configuration of each nanofiber. It is reasonable to assume that the core-shell structure of individual nanofibers may undergo alterations along their length, thereby influencing their piezoelectric response. It is worth highlighting that the proposed composite material presents a piezoelectric response even without a poling process following the electrospinning, likely attributable to two main factors. First, the high electric field used during the electrospinning process induces itself a dipole orientation when the fluid jet comes out from the needle and deposits as nanofibers in the ground collector [45–48]. Moreover, as previously demonstrated in literature, the presence of the conductive PEDOT:PSS core possessing free charges helps the randomly oriented dipoles in the piezoelectric P(VDF-TrFE) shell to align [49].

Furthermore, the absence of any triboelectric contributions was demonstrated by performing the electromechanical tests on the virgin laminate, in which no signals were acquired during the impact events (Section S3 of Supplementary Materials). The embedding of the nanofibers within the epoxy matrix prevents the friction between the two phases, and no triboelectric charges were measured during the impact between the impactor and the surface of the laminate.

Starting from the piezoelectric signals measured for each electrode, it is possible to map the surface of the self-sensing laminate in terms of sensing capability, with the aim to associate each pixel with its sensitivity value. A Pixel Sensitivity Index (PSI) has been introduced as the ratio between the sum of the two signals of the electrodes which geometrically intersect each pixel (ΔV_j and ΔV_k) and the applied force (mV/N), when the pixel itself is mechanically compressed by the indenter. The PSI provides an immediate overview of the sensing surface and could be exploited in the signal conditioning algotithms. When a mechanical impact occurs on a pixel of the laminate surface, for that specific the PSI is defined as follows:

$$PSI_{j,k} = \frac{\left(\Delta V_j + \Delta V_k\right) \pm \sqrt{\sigma_j^2 + \sigma_k^2}}{F} \tag{1}$$

where the subscripts j and k indicate the electrodes on the two edges of the laminate, and σ is the corresponding standard deviation. In particular, the index j refers to ΔV_A, ΔV_B, and ΔV_C, while the index k refers to ΔV_D, ΔV_E, and ΔV_F. In Fig. 11, the PSI are reported for each impacted

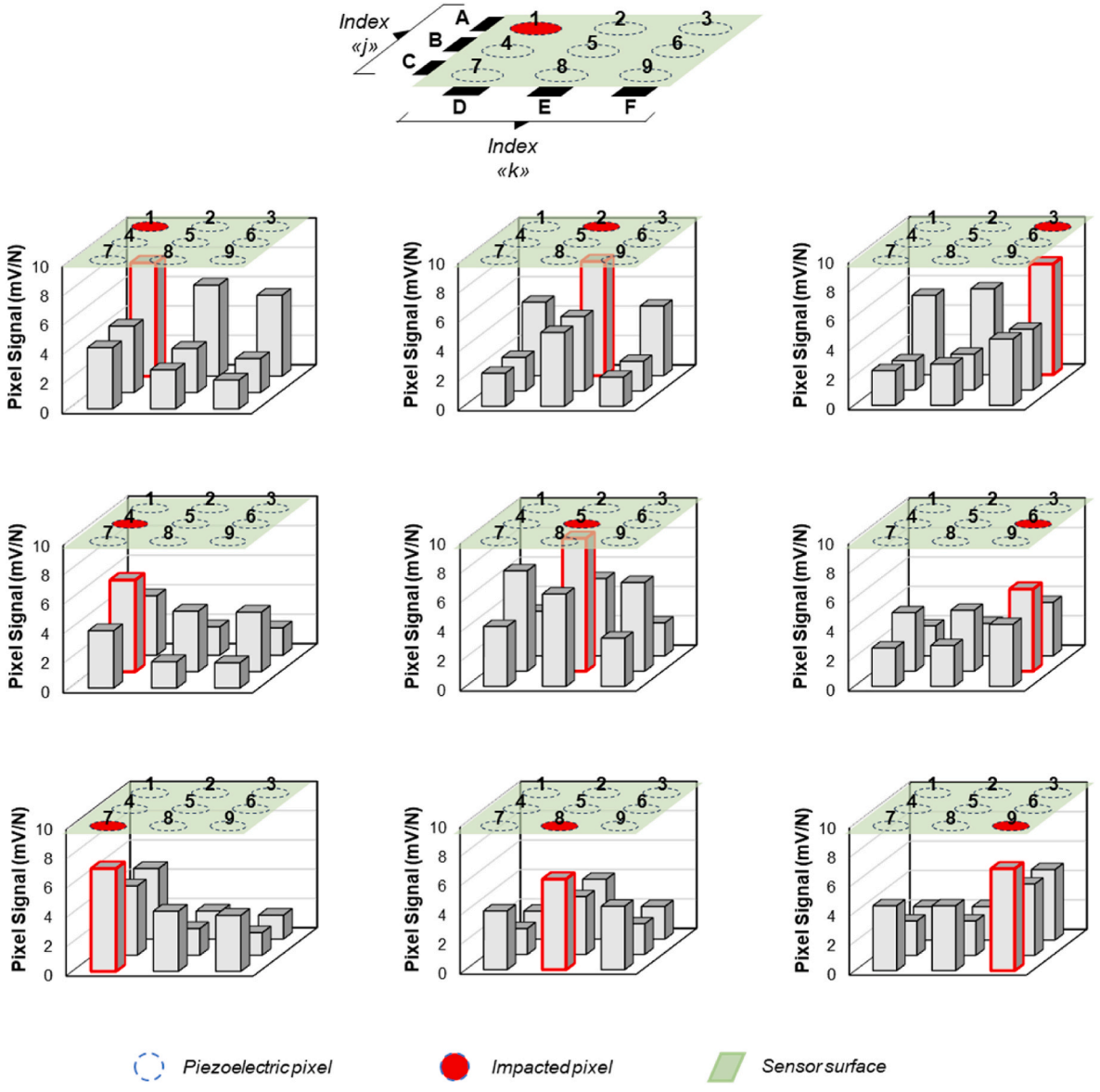

Fig. 11. Sensitivity of each pixel of the composite laminate, represented for each impact position.

position, together with the sensitivities of the not-impacted pixels, which are still defined according to Equation (1). This operation allows for a visual assessment of the sensitivity of each region of the laminate, and could be employed for immediate tactile recognition in real sensing applications. The green areas on the bar graphs in Fig. 11 replicate the square geometry of the sensor, while the red circles indicate the positions of the mechanical impact. The impacted positions are accurately identified by the bars with the highest amplitude (highlighted in red). This representation offers a straightforward overview of the sensitivity distribution across the entire laminate area. When the impact occurs, the two piezoelectric signals associated to the impacted pixel are generated as the result of the compressive force on the piezoelectric phase, and are used to define the corresponding PSI. Conversely, the sensitivities associated to the surrounding not-impacted-pixels are caused by vibrations and elastic waves propagation in the composite matrix. Additionally, inadequate alignment of nanofibers may result in transversal disposition, causing mismatch effects and amplifying the piezoelectric signals in non-impacted pixels. These secondary effects collectively diminish the disparity between the PSI (pertaining to the impacted pixel) and the piezoelectric response in regions of the laminate unaffected by mechanical compression from the indenter. As observable from the graphs of Fig. 10, the piezoelectric signals corresponding to the not-impacted pixels are not negligligle, and their conversion in the graphs of Fig. 11 results in bars which are still comparable with the signal amplitude of the PSI (red bar). However, due to the proper tuning of the coaxial electrospinning and the high alignment grade of the nanofibers interleaved in the composite, in this work the effect of the compression action is preponderant with respect to the other effects. The worst case scenario occurs for the impact on Pixel_1, where the second highest piezoelectric signal is 19.6 % lower than the PSI (7.7 mV/N), and a successful localization was achieved. The average PSI of the impacted piezoelectric pixels (highlighted in red bars) is 7.10 mV/N, with a standard deviation of 0.99 mV/N (13.9 %). In particular, Pixel_5 exhibits the highest PSI (9.04 mV/N), while the lowest PSI is equal to 5.58 mV/N for Pixel_6. According to the experimental findings of this study, this standard deviation value is sufficient for a precise localization and the PSI can define the position of the impact with optimal precision. As aforementioned, the coaxial geometry of each nanofiber plays a crucial role in the sensing mechanism, and achieving lower standard deviation values would result from finer control over the core-shell morphology and the distribution of nanofibers across the sensitive surface of the laminate. Moreover, thanks to the nanometric scale of the of the coaxial fibers, the implementation of sub-micrometric core electrodes stacked on the edges of the laminate would lead to a extremely finer localization capability, with a larger amount of sensitive micro-pixels mapping the composite laminate surface.

4. Conclusions

The composite material proposed in this work embeds piezoelectric core-shell nanofibers (shell of P(VDF-TrFE) and core of PEDOT:PSS), which are exploited for a novel impact localization technique. The sensor comprises a first layer of aligned nanofibers embedded in an epoxy matrix. The second layer is stacked so that its nanofibers are perpendicular to those of the first.

Such a matrix-like disposition generates a pattern of piezoelectric pixels at the intersection of the aligned nanofibers, which are responsible for the detection of an impact on the sensor surface.

By impacting a specific portion of the sensor surface, the amplitude of the measured output voltage corresponding to the impacted pixel was higher than the non-impacted ones. Indeed, the mechanical stress transferred to the piezoelectric nanofibers led to a higher charge generation in that specific region compared to the not-mechanical stressed pixels. In this way, it was possible to localize the impact position by comparing the amplitudes of the output voltages and knowing to which pixel they correspond. A crucial role in the operation of the sensor is given by the core-shell morphology of the nanofibers, which has been expressly tailored as a result of a deep investigation of the interaction between the two coaxially-disposed fluids.

It is noteworthy that the nanofibers do not negatively impact the mechanical performances of the hosting material, and they can be easily integrated into various kinds of polymeric matrices, i.e., silicon-based polymers, to develop flexible structures. This approach can be used to create a sensing network for highly precise mechanical stimuli recognition, and it can be exploited in robotic or biomedical applications.

CRediT authorship contribution statement

Giacomo Selleri: Writing – original draft, Methodology, Investigation, Formal analysis, Conceptualization. **Filippo Grolli:** Methodology, Investigation, Conceptualization. **Maria Roberta Randi:** Writing – original draft, Investigation, Data curation. **Emanuele Maccaferri:** Investigation, Methodology, Writing – review & editing. **Tommaso Maria Brugo:** Supervision, Methodology, Investigation, Formal analysis. **Giovanni Valdrè:** Writing – original draft, Investigation, Data curation. **Andrea Zucchelli:** Writing – review & editing, Writing – original draft, Supervision, Data curation, Conceptualization. **Davide Fabiani:** Writing – review & editing, Writing – original draft, Investigation, Conceptualization.

Declaration of competing interest

The authors declare that they have no known competing financial interests or personal relationships that could have appeared to influence the work reported in this paper.

Data availability

Data will be made available on request.

Acknowledgments

The research was funded by PNR - Alma Idea 2022 (CUP J45F21002000001), by the European Union's Horizon 2020 Research and Innovation Programme – "MyLeg" (No. 780871, 2018) and by Project Ecosyster—Ecosystem for Sustainable Transition in Emilia-Romagna, project funded under the National Recovery and Resilience Plan (NRRP), Award Number: 0001052, (CUP J33C22001240001). The authors would like to thank Solvay and Ddchem S.l.r. for providing the polymers.

Appendix A. Supplementary data

Supplementary data to this article can be found online at https://doi.org/10.1016/j.compositesb.2024.111494.

References

[1] Chung DDL. A review of multifunctional polymer-matrix structural composites. Compos. Part B Eng. 2019;160(November 2018):644–60. https://doi.org/10.1016/j.compositesb.2018.12.117.
[2] Rocha H, Semprimoschnig C, Nunes JP. Sensors for process and structural health monitoring of aerospace composites: a review. Eng Struct 2021;237(July 2020). https://doi.org/10.1016/j.engstruct.2021.112231.
[3] Rim YS, Bae SH, Chen H, De Marco N, Yang Y. Recent Progress in materials and devices toward Printable and flexible sensors. Adv. Mater. 2016;28(22):4415–40. https://doi.org/10.1002/adma.201505118.
[4] Han ST, et al. An overview of the development of flexible sensors. Adv. Mater. 2017;29(33):1–22. https://doi.org/10.1002/adma.201700375.
[5] Pierre Claver U, Zhao G. Recent Progress in flexible pressure sensors based electronic skin. Adv Eng Mater 2021;23(5):1–17. https://doi.org/10.1002/adem.202001187.
[6] Cheng M, et al. A review of flexible force sensors for human health monitoring. J Adv Res 2020;26:53–68. https://doi.org/10.1016/j.jare.2020.07.001.
[7] Wan Y, Wang Y, Guo CF. Recent progresses on flexible tactile sensors. Mater. Today Phys. 2017;1:61–73. https://doi.org/10.1016/j.mtphys.2017.06.002.

[8] Herren B, Saha MC, Liu Y. Carbon Nanotube-based piezoresistive sensors fabricated by Microwave Irradiation. Adv Eng Mater 2020;22(2). https://doi.org/10.1002/adem.201901068.

[9] Pang Y, et al. Epidermis Microstructure inspired graphene pressure sensor with random distributed Spinosum for high sensitivity and large Linearity. ACS Nano 2018;12(3):2346–54. https://doi.org/10.1021/acsnano.7b07613.

[10] Jiang XZ, Sun YJ, Fan Z, Zhang TY. Integrated flexible, Waterproof, Transparent, and self-powered tactile sensing panel. ACS Nano 2016;10(8):7696–704. https://doi.org/10.1021/acsnano.6b03042.

[11] He Z, et al. Capacitive pressure sensor with high sensitivity and Fast response to dynamic interaction based on graphene and porous Nylon networks. ACS Appl Mater Interfaces 2018;10(15):12816–23. https://doi.org/10.1021/acsami.8b01050.

[12] Vijaya MS. Piezoelectric materials and devices applications in engineering and Medical Sciences. 2008.

[13] Cheng J, Qian C, Zhao M, Lee R, Zhang T-Y. Effects of electric fields on the bending behavior of PZT-5H piezoelectric laminates. Smart Mater Struct 2000;9(6):824. https://doi.org/10.1088/0964-1726/9/6/312.

[14] Gino ME, et al. On the design of a piezoelectric self-sensing smart composite laminate. Mater Des 2022;219:110783. https://doi.org/10.1016/j.matdes.2022.110783.

[15] Xin Y, Zhu J, Sun H, Xu Y, Liu T, Qian C. A brief review on piezoelectric PVDF nanofibers prepared by electrospinning. Ferroelectrics 2018;526(1):140–51. https://doi.org/10.1080/00150193.2018.1456304.

[16] Zarei H, Brugo T, Belcari J, Bisadi H, Minak G, Zucchelli A. Low velocity impact damage assessment of GLARE fiber-metal laminates interleaved by Nylon 6,6 nanofiber mats. Compos Struct May 2017;167:123–31. https://doi.org/10.1016/J.COMPSTRUCT.2017.01.079.

[17] Brugo TM, et al. Self-sensing hybrid composite laminate by piezoelectric nanofibers interleaving. Compos. Part B Eng. 2021;212(February):108673. https://doi.org/10.1016/j.compositesb.2021.108673.

[18] Wang X, Sun F, Yin G, Wang Y, Liu B, Dong M. Tactile-sensing based on flexible PVDF nanofibers via electrospinning: a review. Sensors 2018;18(2). https://doi.org/10.3390/s18020330.

[19] Zhi C, Shi S, Si Y, Fei B, Huang H, Hu J. Recent Progress of wearable piezoelectric pressure sensors based on nanofibers, yarns, and their Fabrics via electrospinning. Adv. Mater. Technol. 2022;(October). https://doi.org/10.1002/admt.202201161.

[20] Closson A, Richards H, Xu Z, Jin C, Dong L, Zhang JXJ. Method for Inkjet-printing PEDOT:PSS polymer electrode arrays on piezoelectric PVDF-TrFE fibers. IEEE Sens. J. 2021;XX(XX). https://doi.org/10.1109/JSEN.2021.3071321.

[21] Zhu M, Chng SS, Cai W, Liu C, Du Z. Piezoelectric polymer nanofibers for pressure sensors and their applications in human activity monitoring. RSC Adv 2020;10(37):21887–94. https://doi.org/10.1039/d0ra03293j.

[22] Wang G, et al. Flexible pressure sensor based on PVDF nanofiber. Sensors Actuators, A Phys. 2018;280:319–25. https://doi.org/10.1016/j.sna.2018.07.057.

[23] He Z, Rault F, Lewandowski M, Mohsenzadeh E, Salaün F. Electrospun PVDF nanofibers for piezoelectric applications: a review of the influence of electrospinning parameters on the β phase and crystallinity enhancement. Polymers 2021;13(2):1–23. https://doi.org/10.3390/polym13020174.

[24] Calavalle F, Zaccaria M, Selleri G, Cramer T, Fabiani D, Fraboni B. Piezoelectric and electrostatic properties of electrospun PVDF-TrFE nanofibers and their role in electromechanical Transduction in Nanogenerators and strain sensors. Macromol Mater Eng 2020;305(7):1–8. https://doi.org/10.1002/mame.202000162.

[25] Huang ZM, Zhang YZ, Kotaki M, Ramakrishna S. A review on polymer nanofibers by electrospinning and their applications in nanocomposites. Compos Sci Technol 2003;63(15):2223–53. https://doi.org/10.1016/S0266-3538(03)00178-7.

[26] Kim KB, et al. Transparent and flexible piezoelectric sensor for detecting human movement with a boron nitride nanosheet (BNNS). Nano Energy 2018;54(July):91–8. https://doi.org/10.1016/j.nanoen.2018.09.056.

[27] Eberle G, Bihler E, Eisenmenger W. Polarization Dynamics of VDF-TrFE copolymers. IEEE Trans Electr Insul 1991;26(1):69–77. https://doi.org/10.1109/14.68230.

[28] Chan HLW, et al. Polarization of thick polyvinylidene fluoride/trifluoroethylene copolymer films. J Appl Phys 1996;80(7):3982–91. https://doi.org/10.1063/1.363356.

[29] Selleri G, et al. Study on the polarization process for piezoelectric nanofibrous layers. In: Annu. Rep. - Conf. Electr. Insul. Dielectr. Phenomena, CEIDP, 2021-Decem; 2021. p. 61–4. https://doi.org/10.1109/CEIDP50766.2021.9705470.

[30] Giacometti JA, Fedosov S, Costa MM. Corona charging of polymers: recent advances on constant current charging. Brazilian J. Phys. 1999;29(2):269–79. https://doi.org/10.1590/S0103-97331999000200009.

[31] Ke J-Y, Chu H-J, Hsu Y-H, Lee C-K. A highly flexible piezoelectret-fiber pressure sensor based on highly aligned P(VDF-TrFE) electrospun fibers. Act. Passiv. Smart Struct. Integr. Syst. 2017;10164:101642X. https://doi.org/10.1117/12.2259854. 2017.

[32] Edmondson D, Cooper A, Jana S, Wood D, Zhang M. Centrifugal electrospinning of highly aligned polymer nanofibers over a large area. J Mater Chem 2012;22(35):18646–52. https://doi.org/10.1039/c2jm33877g.

[33] Yee WA, Kotaki M, Liu Y, Lu X. Morphology, polymorphism behavior and molecular orientation of electrospun poly(vinylidene fluoride) fibers. Polymer (Guildf). 2007;48(2):512–21. https://doi.org/10.1016/j.polymer.2006.11.036.

[34] Fabiani D, et al. Nanofibrous piezoelectric structures for composite materials to be used in electrical and electronic components. Proc. Nord. Insul. Symp. 2019;(26):1–5. https://doi.org/10.5324/nordis.v0i26.3263.

[35] Yu H, Huang T, Lu M, Mao M, Zhang Q, Wang H. Enhanced power output of an electrospun PVDF/MWCNTs-based nanogenerator by tuning its conductivity. Nanotechnology 2013;24(40). https://doi.org/10.1088/0957-4484/24/40/405401.

[36] Sharma T, Naik S, Langevine J, Gill B, Zhang JXJ. Aligned PVDF-TrFE nanofibers with high-density PVDF nanofibers and PVDF core-shell structures for endovascular pressure sensing. IEEE Trans Biomed Eng 2015;62(1):188–95. https://doi.org/10.1109/TBME.2014.2344052.

[37] Forward K, Flores A, Rutledge G. Production of core_shell fibers by electrospinning from a free surface _ Elsevier Enhanced Reader.pdf. Chem Eng Sci 2013.

[38] Arras MML, Grasl C, Bergmeister H, Schima H. Electrospinning of aligned fibers with adjustable orientation using auxiliary electrodes. Sci Technol Adv Mater 2012;13(3). https://doi.org/10.1088/1468-6996/13/3/035008.

[39] Lu L, et al. Electrical conductivity investigation of a nonwoven fabric composed of carbon fibers and polypropylene/polyethylene core/sheath bicomponent fibers. Mater Des 2016;112:383–91. https://doi.org/10.1016/j.matdes.2016.09.096.

[40] Choi HJ, Kim MS, Ahn D, Yeo SY, Lee S. Electrical percolation threshold of carbon black in a polymer matrix and its application to antistatic fibre. Sci Rep 2019;9(1):1–12. https://doi.org/10.1038/s41598-019-42495-1.

[41] Persano L, et al. High performance piezoelectric devices based on aligned arrays of nanofibers of poly(vinylidenefluoride-co-trifluoroethylene). Nat Commun 2013;4:1610–33. https://doi.org/10.1038/ncomms2639.

[42] Arrigoni A, Brambilla L, Bertarelli C, Serra G, Tommasini M, Castiglioni C. P(VDF-TrFE) nanofibers: structure of the ferroelectric and paraelectric phases through IR and Raman spectroscopies. RSC Adv 2020;10(62):37779–96. https://doi.org/10.1039/d0ra05478j.

[43] Andrew JS, Clarke DR. Enhanced ferroelectric phase content of polyvinylidene difluoride fibers with the addition of magnetic nanoparticles. Langmuir 2008;24(16):8435–8. https://doi.org/10.1021/la801617q.

[44] Yoo D, Kim J, Kim JH. Direct synthesis of highly conductive poly(3,4-ethylenedioxythiophene):Poly(4-styrenesulfonate) (PEDOT:PSS)/graphene composites and their applications in energy harvesting systems. Nano Res 2014;7(5):717–30. https://doi.org/10.1007/s12274-014-0433-z.

[45] Yousry YM, Yao K, Chen S, Liew WH, Ramakrishna S. Mechanisms for enhancing polarization orientation and piezoelectric parameters of PVDF nanofibers. Adv. Electron. Mater. 2018;4(6):1–8. https://doi.org/10.1002/aelm.201700562.

[46] Ghafari E, Lu N. Self-polarized electrospun polyvinylidene fluoride (PVDF) nanofiber for sensing applications. Compos. Part B Eng. 2019;160(September 2018):1–9. https://doi.org/10.1016/j.compositesb.2018.10.011.

[47] Park S, Kwon Y, Sung M, Lee BS, Bae J, Yu WR. Poling-free spinning process of manufacturing piezoelectric yarns for textile applications. Mater Des 2019;179:107889. https://doi.org/10.1016/j.matdes.2019.107889.

[48] Park J, et al. Ferroelectric polymer nanofibers Reminiscent of Morphotropic phase Boundary behavior for improved piezoelectric energy harvesting. Small 2022;18(15):1–12. https://doi.org/10.1002/smll.202104472.

[49] Han J, et al. Origin of enhanced piezoelectric energy harvesting in all-polymer-based core–shell nanofibers with controlled shell-thickness. Compos. Part B Eng. 2021;223(June):109141. https://doi.org/10.1016/j.compositesb.2021.109141.